Macromolecules

pubs.acs.org/Macromolecules Article

Soluble Polymer Precursors via Ring-Expansion Metathesis Polymerization for the Synthesis of Cyclic Polyacetylene

Zhihui Miao, Debabrata Konar, Brent S. Sumerlin,* and Adam S. Veige*

Cite This: *Macromolecules* 2021, 54, 7840−7848 Read Online

ACCESS | Metrics & More | Article Recommendations | Supporting Information

ABSTRACT: Cyclic polyacetylene (***c*-PA**) is the cyclic derivative of the semiconducting linear polyacetylene. As with the linear derivative, cyclic polyacetylene is insoluble, making its characterization and processing challenging. Herein, we report the synthesis of ***c*-PA** via an indirect approach, employing ring-expansion metathesis polymerization of cyclic alkenes to form soluble polymer precursors. Subsequent retro-Diels−Alder elimination through heating provides ***c*-PA**. Dilute solution characterizations of the polymer precursors including ^{1}H nuclear magnetic resonance spectroscopy, gel permeation chromatography, and infrared and Raman spectroscopy confirm their cyclic structure and, by inference, the cyclic topology of the resulting ***c*-PA**. Solid-state thermal analyses via thermogravimetric analysis and differential scanning calorimetry reveal the chemical and physical transformations occurring during the retro-Diels−Alder elimination step and concurrent isomerization. Freestanding films are attainable via the soluble precursors, and when doped with I_2, the films are semiconducting.

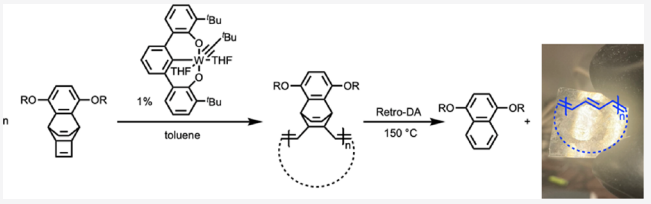

INTRODUCTION

Conjugated polymers possess unique properties including electronic conductivity,[1−5] magnetic susceptibility,[6,7] optical nonlinearity,[8−10] photoconductivity,[11,12] gas permeability,[13−15] and liquid crystallinity.[16,17] Applications of conjugated polymers include sensors, photovoltaics, imaging agents, solar cells, and flexible electronics.[18] However, due to their rigid backbone structure, conjugated polymers often have low solubility and suffer from poor solution processability. For example, the highest performing semiconducting polymers require toxic chlorinated solvents at elevated temperatures for processing.[19,20]

Consisting of a simple hydrocarbon chain with alternating single and double carbon−carbon bonds, polyacetylene (**PA**) has been the model polymer for studying the effects of conjugation. However, with its rigid conformation, **PA** exhibits extremely poor solubility in any solvent, severely limiting its processability. Notably, Natta et al.[21] first synthesized **PA** from acetylene gas with titanium-based catalysts in 1958, producing an insoluble black solid with no clear melting point. Characterization of such a material was impossible at the time. Almost 20 years later, **PA** stoked renewed interest when Shirakawa et al. synthesized freestanding films of linear **PA** with a metallic appearance.[22,23] Subsequently, Heeger et al. discovered that after doping with halogen vapor, **PA** films exhibited conductivities that are comparable to metals.[24] Investigation of **PA** bloomed, but its notorious insolubility continues to limit solution characterization, processability, and application.

In addition to directly synthesizing **PA** solids from acetylene gas, there are indirect routes to prepare **PA** via the transformation of soluble polymeric precursors. Two approaches via precursor transformation are isomerization from nonconjugated polymers to **PA** and producing **PA** through the elimination of small molecules from a nonconjugated polymer precursor. Grubbs et al. demonstrated the transformation of soluble polybenzvalene to **PA** via isomerization (Figure 1A).[25] Ring-opening metathesis polymerization (ROMP) of benzvalene with a tungsten alkylidene catalyst produces polybenzvalene, a soluble **PA** precursor. Polybenzvalene, upon treating with $HgCl_2$ in THF, isomerizes to insoluble **PA** without mass loss, though severe mechanical stress or rapid heating induces exothermic decomposition.[25] Similarly, Xia et al., in 2017, reported the synthesis of **PA** from a soluble polyladderene precursor by mechanical forces (Figure 1B).[26] Polymerizing a ladderene monomer via ROMP with Grubbs' catalyst yields a soluble, colorless polymer. *trans*-**PA** of uniform conformation and long conjugation length forms upon sonicating the nonconjugated soluble polyladderene precursor.[26] Applying this mechanochemical transformation method to other ladderene polymers yields acetylene copolymers,[27,28] including fluorinated polyacetylene.[29] Bielawski et al. also prepared *trans*-**PA** from a masked polymer of Dewar benzene via isomerization (Figure 1C).[30] **PA** forms via a polymerization−

Received: April 30, 2021
Revised: August 13, 2021
Published: September 1, 2021

Downloaded via FLORIDA STATE UNIV on January 8, 2025 at 21:46:43 (UTC).
See https://pubs.acs.org/sharingguidelines for options on how to legitimately share published articles.

ACS Publications © 2021 American Chemical Society

https://doi.org/10.1021/acs.macromol.1c00938
Macromolecules 2021, 54, 7840−7848

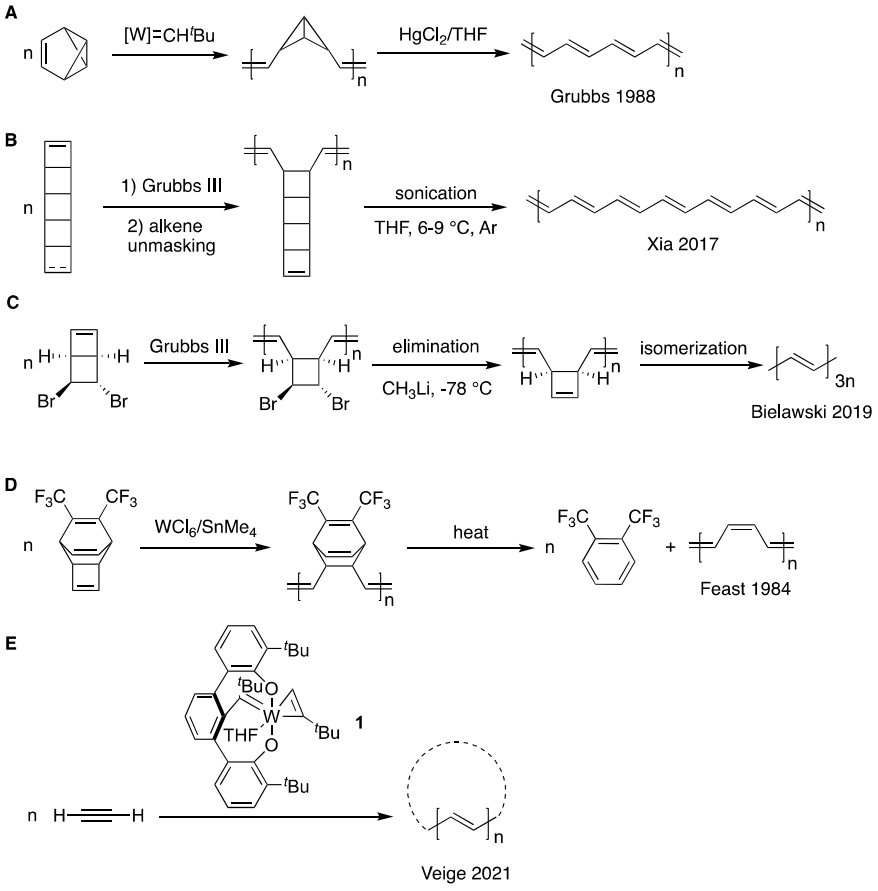

Figure 1. (A–E) Selected approaches for **PA** synthesis.

Scheme 1. Synthesis of Monomers M1–M3

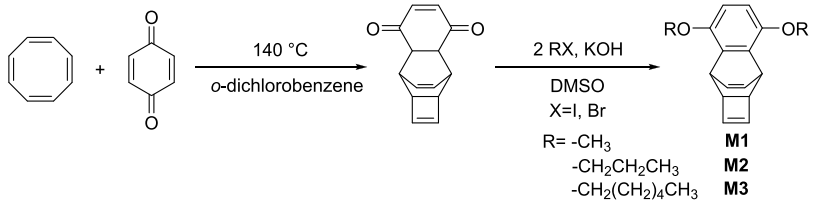

elimination–isomerization sequence; however, the Dewar monomer requires a complicated multistep synthesis and purification.

Eliminating a small molecule from a non-conjugated polymer precursor to form **PA** is another indirect method. The method involves the polymerization of monomers that consist of tricyclo-decatriene units, one being cyclobutene, a vulnerable group toward ROMP. Retro-[4+2]cycloaddition or the "retro-Diels–Alder" reaction produces **PA** from the soluble polymers upon heating (Figure 1D).[31−33] Eliminating benzene or substituted benzene molecules is the driving force for the reaction. However, most of these soluble polymer precursors are not stable and self-eliminate benzene(s) at room temperature, particularly the CF_3-disubstituted precursor.[31,32] Affording improved characterization and good samples of **PA**, precursors bearing naphthalene units are soluble and stable at room temperature.[32]

Cyclic polyacetylene (***c*-PA**)[34] is now accessible from acetylene gas and catalyst **1**[35−37] (Figure 1E), but the relationships between its cyclic topology and physical, electronic, and mechanical properties are unknown. Smaller hydrodynamic volumes, lower intrinsic and melt viscosities, and higher glass transition temperatures (T_g) are properties that differ between linear and cyclic polymers.[36,38−42] Potentially more conjugated, and therefore more conductive, cyclic polymers have fewer degrees of freedom due to their inherent topological constraint.[43] However, previous studies have suggested more limited conjugation lengths for cyclic polymers that could arise from segment bending/torsion, possibly mitigating cyclic topology effects on conductivity.[44,45] Nevertheless, attributable to a low-energy isomerization barrier for the ring structure, ***c*-PA** contains >99% *trans* double bonds. After doping, ***c*-PA** exhibits conductivity on the higher end of doped ***l*-PA** (without chain alignment).[46,47] Thus, there is still an ambiguity over the effect of cyclic topology on the conductivity that needs further investigation. Providing evidence of a cyclic structure remains challenging due to the insoluble nature of **PA**. Atomic force microscopy (AFM) images of cyclic bottlebrush derivatives of ***c*-PA** provide absolute evidence for the cyclic topology.[34,48] Another approach to confirming the cyclic topology is to first synthesize a soluble precursor and execute solution-phase structural

https://doi.org/10.1021/acs.macromol.1c00938
Macromolecules 2021, 54, 7840−7848

investigations prior to forming *c*-**PA**. Herein, we report the ring-expansion metathesis polymerization (REMP) of cyclic alkenes via tungsten alkylidyne catalyst **2**[49,50] to yield soluble cyclic polymer precursors to *c*-**PA**. Accessible now from a soluble and processable polymer precursor are lustrous thin films of *c*-**PA** that exhibit high conductivity when doped.

RESULTS AND DISCUSSION

Scheme 1 depicts the general preparation of benzotricyclodecatriene monomers **M1**−**M3**. Performing a Diels−Alder reaction of cyclooctatetraene and benzoquinone generates cyclobutanaphthalene-4,7-dione on a multigram scale. Altering the chain length of the aryl-ether via O-alkylation alters the solubility of the resulting polymers.

Scheme 2 depicts the synthesis of soluble cyclic polymer precursors to **c-PA**. As reported previously, tungsten alkylidyne

Scheme 2. Synthesis of Soluble Cyclic Polymer Precursors to c-PA

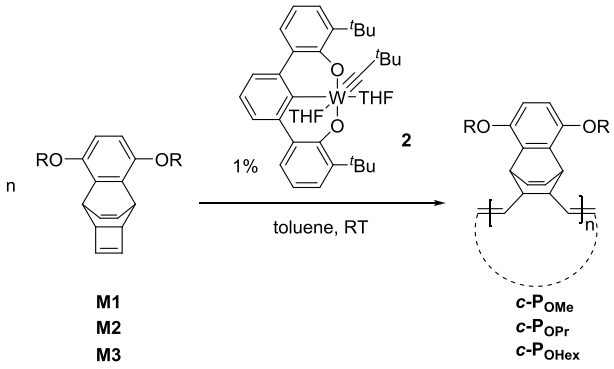

catalyst **2** initiates the polymerization of norbornene to cyclic polynorbornene via REMP,[50] but this is the first disclosure of its activity with a monomer containing a cyclobutene moiety. Treating toluene solutions of the monomers with 1 mol % **2** initiates REMP; the solutions change color from light red/orange (catalyst color) to green. For the 2a,3,8,8a-tetrahydro-4,7-dimethoxy-3,8-ethenocyclobuta[b]naphthalene (R = Me, **M1**) and 2a,3,8,8a-tetrahydro-4,7-dipropoxy-3,8-ethenocyclobuta[b]naphthalene (R = Pr, **M2**) monomers, the reaction solution turns cloudy within 30 min, and white solids precipitate. For the 2a,3,8,8a-tetrahydro-4,7-dihexoxy-3,8-ethenocyclobuta[b]naphthalene (R = Hex, **M3**) monomer, the solution remains homogeneous and turns yellow as the polymerization proceeds. Monitoring the polymerization via ^{1}H NMR spectroscopy (C_6D_6) reveals the activity of **2**. During polymerization, the resonances from the **M1** monomer slowly decrease, and the conversion reaches 82% within 2 h and 96% after 24 h. During this time, no obvious polymer resonances appear in the NMR spectra, indicating that the polymer is not soluble in C_6D_6. REMP of **M2** was slower, reaching 69% conversion in 2 h and 98% after 24 h. For the REMP of **M2**, minor broad resonances appear after 24 h in the ^{1}H NMR spectrum of the reaction mixture, indicating higher polymer solubility. **M3** polymerizes the slowest, reaching 53% conversion after 24 h. The REMP of **M3** produces a polymer (*c*-$\mathbf{P}_{\mathbf{OHex}}$) that was more soluble in C_6D_6 relative to the polymers from the REMP of **M1** (*c*-$\mathbf{P}_{\mathbf{OMe}}$) and **M2** (*c*-$\mathbf{P}_{\mathbf{OPr}}$); very few solids precipitate during polymerization, and broad resonances appear in the ^{1}H NMR spectra. The solubility increase of *c*-$\mathbf{P}_{\mathbf{OHex}}$ may be due to the longer alkyl groups.

Additional support for the successful REMP of **M3** comes from infrared spectroscopy (Figure 2). The C═C stretch at 1552

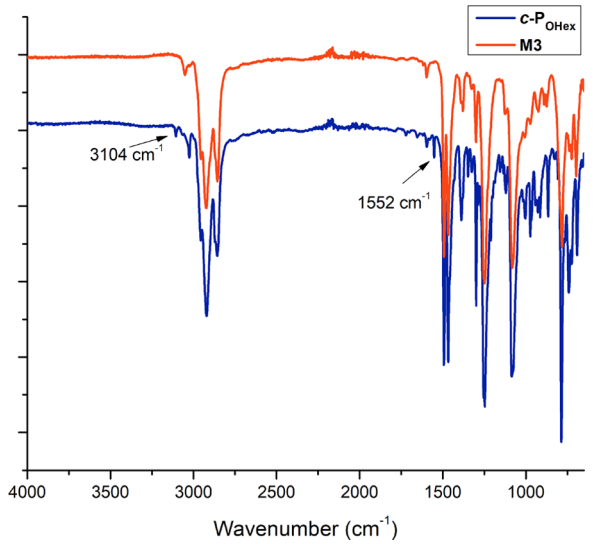

Figure 2. Infrared spectra of the **M3** monomer (orange) and *c*-$\mathbf{P}_{\mathbf{OHex}}$ (blue). Highlighted is the disappearance of absorptions at 1552 (C═C of cyclobutene) and 3104 cm^{-1} (═C−H of cyclobutene) indicating successful ring opening of the cyclobutene unit.

cm^{-1} and the ═C−H stretch at 3104 cm^{-1} of the cyclobutene unit[32] of **M3** both disappear after polymerization. Comparing IR spectra of **M1** and **M2** with their respective polymers (Figures S2 and S4) also reveals the loss of these signals, suggesting successful REMP of all monomers.

Ring-opening metathesis polymerization (ROMP) of monomers **M1**, **M2**, and **M3** using Hoveyda-Grubbs second generation catalyst yields linear polymers *l*-$\mathbf{P}_{\mathbf{OMe}}$, *l*-$\mathbf{P}_{\mathbf{OPr}}$, and *l*-$\mathbf{P}_{\mathbf{OHex}}$, respectively (Scheme 3). Similar to REMP of **M1**−**M3**,

Scheme 3. Synthesis of Linear Polymer Precursors

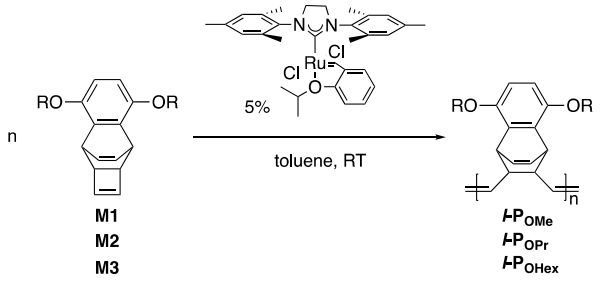

the linear polymers *l*-$\mathbf{P}_{\mathbf{OMe}}$ and *l*-$\mathbf{P}_{\mathbf{OPr}}$ are relatively insoluble, whereas *l*-$\mathbf{P}_{\mathbf{OHex}}$ is readily soluble in THF. The disappearance of the cyclobutene C═C and ═C−H stretching vibrations in the IR spectra of the linear polymers (Figures S1, S3, and S5) confirms successful ROMP. Limiting solution characterization via gel permeation chromatography (GPC), static light scattering (SLS), and viscometry, the low solubility of both cyclic and linear $\mathbf{P}_{\mathbf{OMe}}$ and $\mathbf{P}_{\mathbf{OPr}}$ prevents their topology assignment. Amenable to GPC with SLS analysis, however, *c*-$\mathbf{P}_{\mathbf{OHex}}$ has a number-average molecular weight (M_n) of 100,800 Da with a dispersity ($Đ$) of 1.23, and *l*-$\mathbf{P}_{\mathbf{OHex}}$ has an M_n of 137,400 Da and $Đ$ = 1.06 (Figures S6 and S7).

GPC, coupled with SLS and viscometry detection, reveals the topological differences between soluble *c*-$\mathbf{P}_{\mathbf{OHex}}$ and *l*-$\mathbf{P}_{\mathbf{OHex}}$.

https://doi.org/10.1021/acs.macromol.1c00938
Macromolecules 2021, 54, 7840−7848

Compared to linear analogs with similar molecular weights, the hydrodynamic radii of cyclic polymers are smaller.[51] Therefore, cyclic polymers have longer retention times on GPC, making this approach a reliable method for distinguishing between the topologies.[52] Figure 3 depicts the log (molar mass) versus

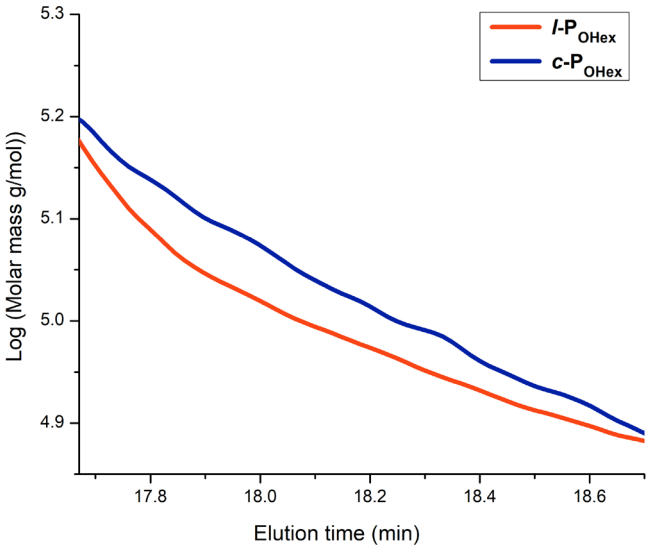

Figure 3. Log (molar mass) versus elution time for ***c*-P$_{OHex}$** and ***l*-P$_{OHex}$** by GPC in THF at 35 °C.

elution time plot for ***c***- and ***l*-P$_{OHex}$**. At any given molecular weight, ***c*-P$_{OHex}$** elutes later, revealing its smaller size and, by inference, its cyclic topology.

Intrinsic viscosity $[\eta]$ data provide additional evidence for the cyclic topology of ***c*-P$_{OHex}$**. Figure 4 depicts the Mark–Houwink–Sakurada (MHS) plot comparing the intrinsic viscosity of ***c*-P$_{OHex}$** and ***l*-P$_{OHex}$** as a function of molar mass. As a consequence of the absence of chain entanglements and a smaller radius of gyration in solution, cyclic polymers exhibit smaller intrinsic viscosities than their linear analogs.[53] The

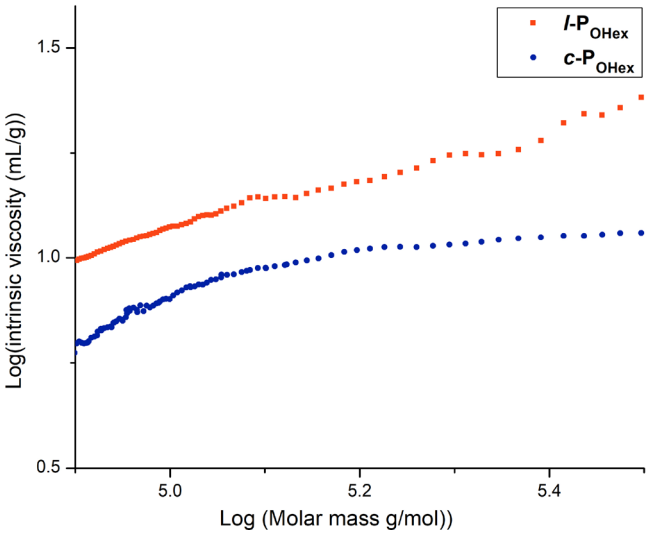

Figure 4. Mark–Houwink–Sakurada plot comparing intrinsic viscosity $[\eta]$ over a range of molar masses for ***c*-P$_{OHex}$** and ***l*-P$_{OHex}$** obtained by GPC in THF at 35 °C, indicating that ***c*-P$_{OHex}$** has lower intrinsic viscosity than ***l*-P$_{OHex}$**.

overall observed $[\eta]_{average,\ cyclic}/[\eta]_{average,\ linear}$ ratio is 0.651, a very close fit to the theoretical value 0.658.[54] Moreover, over a broad range of molecular weights, from 7.9×10^4 to 3.1×10^5 Da, the ratio of $[\eta]_{cyclic}/[\eta]_{linear}$ holds closely to the theoretical value, suggesting a high topological purity for ***c*-P$_{OHex}$**. Further, the MHS *a* values for ***c*-P$_{OHex}$** and ***l*-P$_{OHex}$** are 0.870 and 0.797, respectively, indicating that both polymers behave similarly as semiflexible in THF under ambient conditions.

Subsequent transformation of cyclic polymer precursors to ***c*-PA** only requires the elimination of pendent naphthalene (Scheme 4) without interrupting the backbone, thus retaining

Scheme 4. Formation of *c*-PA from Soluble Polymer Precursors via a Retro-Diels–Alder Reaction

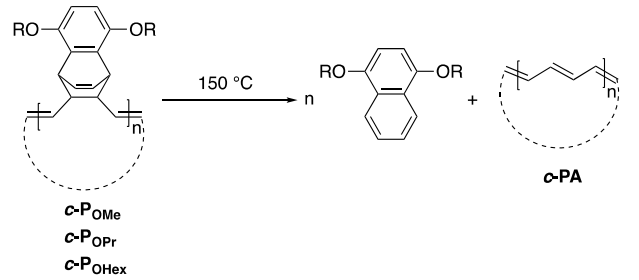

the intrinsic cyclic topology. The precursors self-eliminate substituted naphthalene over prolonged storage; ^{1}H NMR spectra of the polymers stored at room temperature in the dark for a month exhibit resonances from substituted naphthalene molecules. The polymers change color from white to orange to red and then to black, over a few weeks, indicating self-elimination and a progressively increasing conjugated backbone.

Heat promotes the elimination reaction to generate **PA**.[32] Heating the polymers in a N_2-filled vial at 150 °C turns the solids from red to black within 5 min with concomitant off-white solids forming on the polymer surface. Subsequent sublimation removes the white solids (naphthalenes). After 30 min of heating, washing the black polymer solids with THF and pentane removes residual naphthalene, and weight loss data indicate an elimination yield of >96%.

Heating a C_6D_6 solution of ***c*-P$_{OHex}$** at 70 °C in an NMR probe and obtaining spectra periodically reveal the elimination reaction. Assigned to the backbone double bond protons on ***c*-P$_{OHex}$**, the initial ^{1}H NMR spectrum of the precursor polymer exhibits a broad resonance at 5.5 ppm. Attributable to 1,4-bis(hexyloxy)naphthalene, sharp resonances appear at 8.24 and 7.49 ppm over time, confirming successful elimination. Complete ^{1}H NMR spectral assignments are provided in the Supporting Information.

Thermal gravimetric analysis (TGA) of ***c*-P$_{OHex}$** reveals two weight loss processes during heating (Figure 5, orange trace). The first transition, with an onset temperature of 100 °C, accounts for 84% of the total mass, a close fit to the molar mass ratio (87%) for 1,4-bis(hexyloxy)naphthalene to the repeating unit. The second transition with an onset temperature of 256 °C is the decomposition of ***c*-PA** that forms during the first thermal event; the trace fits well with the decomposition of pure ***c*-PA** (Figure 5, blue trace), with the weight loss (56% of the remaining) being a close fit to the weight loss observed in the TGA of pure ***c*-PA**(63%).[34] In the same vein, TGA of ***c*-P$_{OMe}$** revealed two distinct transitions, corresponding to 73% of the total mass loss at 100 °C and 60% of the remaining mass

https://doi.org/10.1021/acs.macromol.1c00938
Macromolecules 2021, 54, 7840–7848

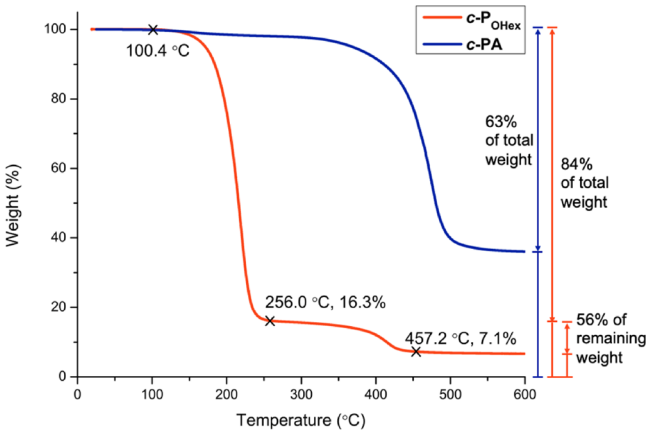

Figure 5. TGA traces of *c*-$\mathbf{P_{OHex}}$ (orange) and directly synthesized *c*-**PA** (blue).

loss at 392 °C. These transitions fit well to the molar mass ratio (78%) of 1,4-bis(methoxy)naphthalene to the repeat unit and the decomposition of ***c*-PA**, respectively (Figure S17). Moreover, evolved gas analysis using TGA coupled with a mass spectrometer (TGA-MS) of *c*-$\mathbf{P_{OMe}}$ shows the emergence of molecular ion (M^+) and (M+1) peaks, corresponding to 1,4-bis(methoxy)naphthalene and its associated mass fragments (Figure S19). This further solidifies the claim for the elimination of naphthalene moieties leading to the generation of ***c*-PA**.

Feast et al. studied similar soluble linear precursors and monitored the conversion to ***l*-PA** via differential scanning calorimetry (DSC).[31] Their DSC scans contain two well-separated exotherms. Eliminating 1,2-bis(trifluoromethyl)-benzene from the polymer backbone is the first exothermic event, and isomerization of the resulting *cis*-***l*-PA** to the more thermodynamically stable *trans* configuration is the second event.[31]

Direct synthesis of ***c*-PA** from acetylene via ring-expansion polymerization using a tungsten alkylidene catalyst according to Figure 1E yields exclusively *trans*-***c*-PA**.[34] In contrast, $AlEt_3$/$Ti(O^nBu)_4$ produces *cis*-***l*-PA**.[23] Obtaining the more stable *trans* linear isomer requires heating. The cyclic topology of ***c*-PA** facilitates isomerization via a low barrier to π bond shifting and single bond rotation within the ring. DSC traces of ***l*-**$\mathbf{P_{OMe}}$ and ***c*-**$\mathbf{P_{OMe}}$ (Figure 6) reveal differences that are attributable to the distinct topologies. Revealing a topological difference, the DSC trace of ***c*-**$\mathbf{P_{OMe}}$ reveals a lower temperature (~70 °C) for the onset of naphthalene elimination. More obvious is the simultaneous elimination and the onset of *cis*−*trans* isomerization at a significantly lower temperature of ~90 °C and a broader trace leading to a peak at 132 °C for the *cis*−*trans* isomerization. The DSC trace of ***l*-**$\mathbf{P_{OMe}}$ reveals an onset for elimination at ~90 °C and a maximum at ~110 °C for the *cis*−*trans* isomerization. These differences are attributable to the cyclic versus linear topology. However, while monitoring the generation of **PA** from cyclic and linear $\mathbf{P_{OHex}}$ via DSC, the two traces (Figures S20 and S21) both reveal broad peaks centered at ~140 °C, in close agreement to the *cis*−*trans* isomerization temperature that Feast et al. observed.[31] The similar maximum near 140 °C for both linear and cyclic polymers is consistent with disruption of conjugation; the few remaining double bonds isomerizing at that temperature do not benefit from the topology difference.

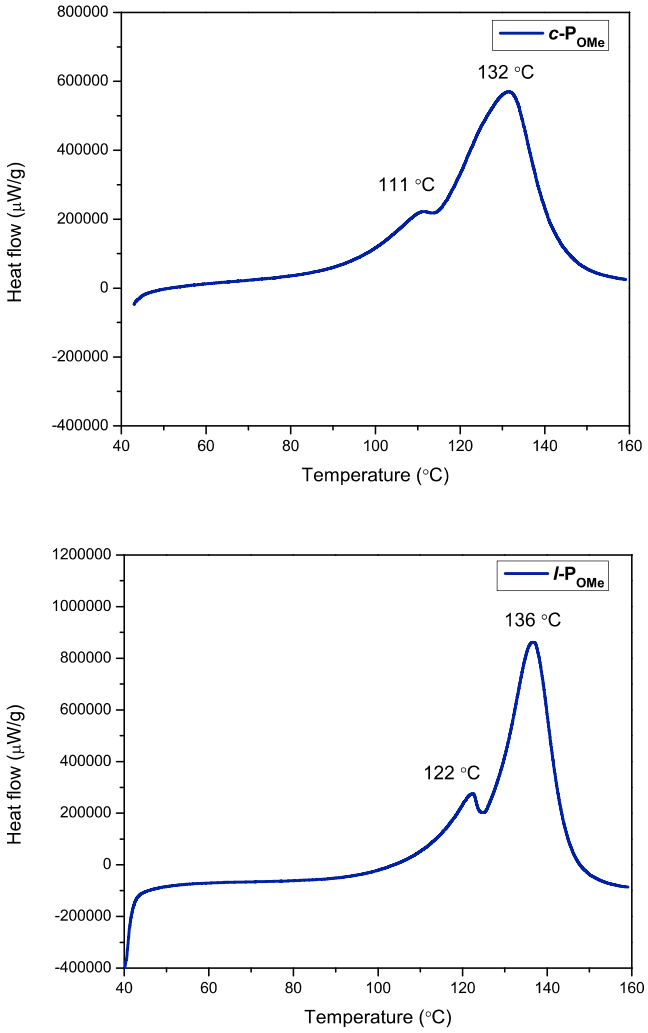

Figure 6. DSC traces of cyclic (top) and linear (bottom) $\mathbf{P_{OMe}}$.

IR spectra (Figure 7) of the final **PA** products, from both the cyclic and linear precursors, indicate the *trans*−*transoid* nature of both polymers, with strong *trans* =C—H out-of-plane bending around 1000 cm^{-1}. There are minor absorptions around 728 cm^{-1} that are attributable to *cis* =C—H out-of-plane bending[23] or minor uneliminated segments. Raman spectra and solid-state cross-coupling magic angle spinning (CP-MAS) ^{13}C NMR spectral data complement the IR spectral data and the assignment of highly *trans* polymers.

Raman spectra (Figure 8) of ***c*-** and ***l*-PA** both exhibit absorptions near 1500 cm^{-1} when excited with 785 and 633 nm lasers, indicating a *trans*−*transoid* conformation for both polymers. Importantly, the Raman spectra of ***c*-PA** and ***l*-PA** lack the distinct absorptions for *cis* conformations, whereas the Raman spectrum for directly synthesized linear *cis*-**PA** exhibits signals at 920, 1250, and 1550 cm^{-1}.[55,56] The absence of these *cis*-specific absorptions for ***c*-** and ***l*-PA** in this study, especially the strong and sharp signal at 1250 cm^{-1}, indicates that **PA** from $\mathbf{P_{OHex}}$ exhibits a highly *trans* conformation. This is not surprising as heating is a common *cis*-to-*trans* isomerization method for **PA**.[23] The Raman frequency of the C=C stretch in *trans*-**PA** is also an indicator of the conjugation length. Several studies correlate the Raman frequency of *trans* C=C stretching to the conjugation length, either via extrapolations from oligomers[56−59] or calculations using different theoretical

https://doi.org/10.1021/acs.macromol.1c00938
Macromolecules 2021, 54, 7840−7848

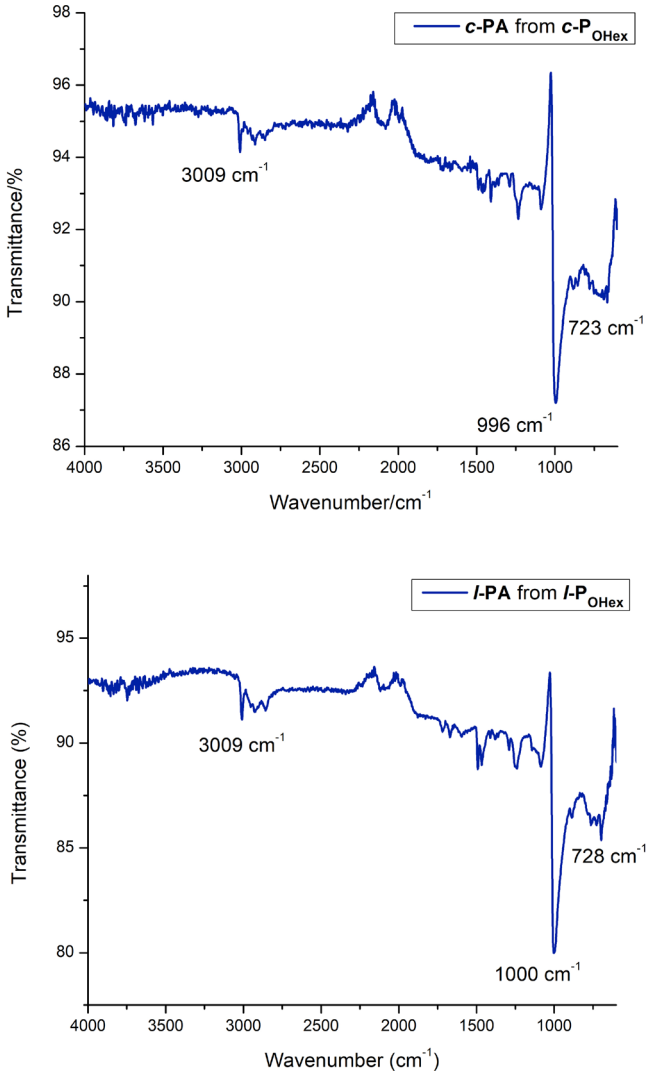

Figure 7. Infrared spectra of **PA** generated from cyclic (top) and linear (bottom) $\mathbf{P}_{\mathbf{OHex}}$ via retro-Diels–Alder reactions.

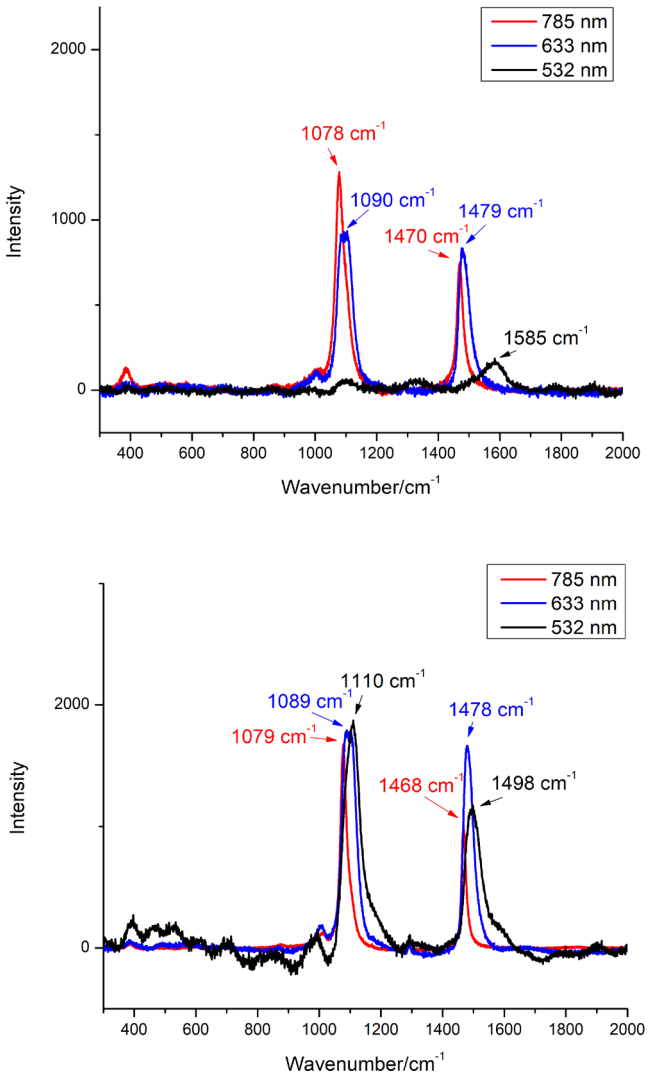

Figure 8. Raman spectra of **PA** from cyclic (top) and linear (bottom) $\mathbf{P}_{\mathbf{OHex}}$ via retro-Diels–Alder reactions, with 785, 633, and 532 nm excitation lasers.

studies.[60,61] Inputting the value of the absorptions for ***c*-PA** and ***l*-PA** into the equations from those computational studies[57−59,61] (see the SI) reveals an average conjugation length of 20−30, a close fit to the reported values of linear **PA** from soluble precursors.[31]

In agreement with the Raman study, solid-state CP-MAS ^{13}C NMR spectroscopy (Figure 9) of the resulting black solids from heat treatment of ***l*-P$_{OHex}$** and ***c*-P$_{OHex}$** also reveals their *trans*-**PA** identity with resonances centered at 136 ppm. Besides resonances from *trans* C═C, both ***c*-PA** and ***l*-PA** exhibit multiple resonances from 10 to 60 ppm, at 68, 106, and 148 ppm, and shoulders of the main *trans* C═C around 120−130 ppm due to a small portion of uneliminated segments in the resulting polymers and 1,4-bis(hexyloxy)naphthalene trapped in the polymers. Resonances of the eliminated 1,4-bis(hexyloxy)naphthalene in a solution-phase ^{13}C NMR spectrum align well with the extra signals in the CP-MAS ^{13}C NMR spectra of ***c*-PA** and ***l*-PA** (see Figure S33 with the overlapped spectra), thus supporting the claim of trapped 1,4-bis(hexyloxy)naphthalene.

Previously reported MAS-DNP ^{13}C NMR spectra of directly synthesized ***c*-PA** and ***l*-PA** exhibit a clear difference in the broadness of their *trans* C═C resonances, with ***c*-PA** having a

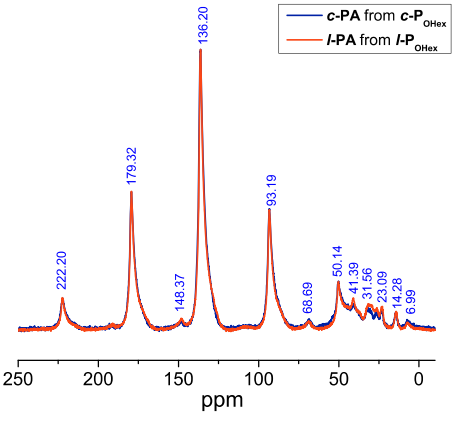

Figure 9. Solid-state CP-MAS ^{13}C NMR spectra of resulting ***c*-PA** (blue) and ***l*-PA** (orange) from ***c*-P$_{OHex}$**, and ***l*-P$_{OHex}$**, respectively.

~3 ppm broader width at half-height, possibly attributable to the cyclic topology.[34] The CP-MAS spectrum of ***c*-PA** generated from ***c*-P$_{OHex}$** also exhibits a slightly broader (~1 ppm at half-height) resonance for the *trans* C═C compared to

https://doi.org/10.1021/acs.macromol.1c00938
Macromolecules 2021, 54, 7840−7848

the *l*-**PA** analog. Considering that both *c*-**PA** and *l*-**PA** are from parent soluble precursors with similar molecular weights via the same thermal treatment, it is likely that the broadness difference comes from their topological difference. Studies are ongoing to confirm this phenomenon.

Solvent-casting cyclic and linear $\mathbf{P}_{\mathbf{OHex}}$ in THF affords thin films of both precursors that turn black upon heating at 150 °C under an inert gas atmosphere (Figure 10). Interestingly, the

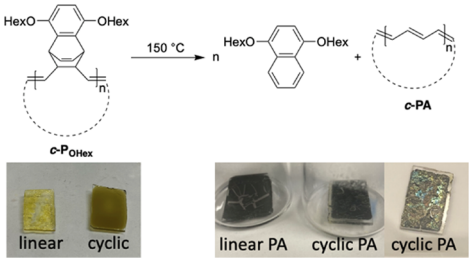

Figure 10. Films of linear and cyclic $\mathbf{P}_{\mathbf{OHex}}$ generated via solvent-casting (left) and the resulting linear and cyclic **PA** after heating (right). The difference in lustrous appearance is due to a viewing angle difference.

linear polymer film breaks into smaller pieces, while the cyclic polymer suffers only cracking within the film and remains whole. Washing with THF and allowing the films to dry remove elimination products and afford purified films. The conductivity of each film is below the measuring limit of a 4-point-probe station (10^{-6} Ω^{-1} cm^{-1}). However, doping the films with I_2 for 3 h produces conductive films. Table 1

Table 1. Conductivity of Cyclic Polyacetylene and Linear Polyacetylene Generated from Cyclic and Linear $\mathbf{P}_{\mathbf{OHex}}$, Respectively

sample	composition	conductivity
c-**PA** from *c*-$\mathbf{P}_{\mathbf{OHex}}$	$(CHI_{9.4})_n$	0.82 Ω^{-1} cm^{-1}
l-**PA** from *l*-$\mathbf{P}_{\mathbf{OHex}}$	$(CHI_{10.2})_n$	0.12 Ω^{-1} cm^{-1}

summarizes their conductivities. The *c*-**PA** and *l*-**PA** films exhibit similar conductivities. This is not surprising as their precursors have similar molecular weights and dispersities. However, the conductivities are much lower than those of directly synthesized *c*-**PA** and *l*-**PA** materials.[4,34] A consequence of the shorter straight-chain structures, more conformational defects, and, thus, higher π–π^* band gap in their materials, Feast et al. also observed lower conductivities for their indirectly generated *l*-**PA** compared to Shirakawa.[31] An additional reason for the lower conductivities might be the purity of the **PA** post-elimination. Further, the conductivity of synthesized undoped *c*-**PA** (10^{-6} Ω^{-1} cm^{-1}) is in close agreement with the electrical conductivity of indirectly generated *l*-**PA** reported by Bielawski et al. via isomerization (10^{-4} Ω^{-1} cm^{-1})[30] and by Feast et al. via elimination (10^{-8} Ω^{-1} cm^{-1}).[31] IR spectra indicated saturated segments in both the cyclic and linear materials corresponding with C_{sp3}–H stretching below 3000 cm^{-1}, possibly due to residual uneliminated naphthalene units or saturation occurring within **PA** as a result of heating given its high reactivity, or both.

CONCLUSIONS

By coupling the solubility benefits conferred from soluble precursors with innovations in catalyst design for REMP, *c*-**PA** is now accessible by indirect synthesis. This strategy provides an easy approach for *c*-**PA** synthesis that is comparable to other well-established REMP catalysts and monomers. The soluble cyclic polymer precursors have the benefit of permitting solution characterizations and thus enable the measurement of MW and $Đ$, whereas the user is blind to these metrics when generating **PA** from acetylene directly. With the possibility to tune the size of the precursor polymers, varying the molecular weight-related properties of the resulting *c*-**PA** will be easy to manage. Topological effects are beginning to emerge in the synthesis of conjugated polymers. Presented in this work are the clearly lower temperatures for the onset of elimination and *cis*–*trans* isomerization. Processing **PA** is a longstanding challenge. Indirect synthesis using soluble precursors offers the chance to exploit the interesting properties of **PA** and potentially manipulate device fabrication. Now that an efficient synthesis is available for *c*-**PA** from acetylene (Figure 1E),[34] the soluble precursor method established in this work bears more importance since elucidating topological differences within **PA** will undoubtedly require matching MW and $Đ$ to historical samples, something not currently possible. Glimpses of topological differences are beginning to appear in the data such as the broader ^{13}C NMR spectral signals and lower onset temperature of elimination. The conjugation length is central to any discussion of **PA** and conductivity. Future studies aim to unravel the possibility that a cyclic topology presents an inherently more conjugated polymer, studies that undoubtedly will rely on controllable soluble precursors.

ASSOCIATED CONTENT

Supporting Information

The Supporting Information is available free of charge at https://pubs.acs.org/doi/10.1021/acs.macromol.1c00938.

Full experimental procedures, NMR spectra, IR spectra, Raman spectra, DSC traces, TGA traces, and GPC traces (PDF)

AUTHOR INFORMATION

Corresponding Authors

Brent S. Sumerlin − *George & Josephine Butler Polymer Research Laboratory, Center for Macromolecular Science & Engineering, Department of Chemistry, University of Florida, Gainesville, Florida 32611, United States;* orcid.org/0000-0001-5749-5444; Email: sumerlin@chem.ufl.edu

Adam S. Veige − *Center for Catalysis, Department of Chemistry and George & Josephine Butler Polymer Research Laboratory, Center for Macromolecular Science & Engineering, Department of Chemistry, University of Florida, Gainesville, Florida 32611, United States;* orcid.org/0000-0002-7020-9251; Email: veige@chem.ufl.edu

Authors

Zhihui Miao − *Center for Catalysis, Department of Chemistry and George & Josephine Butler Polymer Research Laboratory, Center for Macromolecular Science & Engineering, Department of Chemistry, University of Florida, Gainesville, Florida 32611, United States*

Debabrata Konar − *George & Josephine Butler Polymer Research Laboratory, Center for Macromolecular Science & Engineering, Department of Chemistry, University of Florida, Gainesville, Florida 32611, United States*

Complete contact information is available at:
https://pubs.acs.org/10.1021/acs.macromol.1c00938

Author Contributions

Z.M. synthesized cyclic and linear $\mathbf{P}_{OMe}$, $\mathbf{P}_{OPr}$, and P; generated cyclic and linear polyacetylene from $\mathbf{P}_{OMe}$, $\mathbf{P}_{OPr}$, and $\mathbf{P}_{OHex}$; characterized the polymerization and soluble polymers via NMR spectroscopy, $\mathbf{P}_{OMe}$ and P via DSC and TGA, all the polymers via IR spectroscopy, and all polyacetylene via Raman spectroscopy; doped polyacetylene; and measured the conductivities. D.K. synthesized, purified, and characterized the monomers M1−M3 and characterized the cyclic and linear $\mathbf{P}_{OHex}$ via GPC, SLS, and solution viscometry and $\mathbf{P}_{OMe}$ via TGA-MS. The manuscript was written through contributions of all authors. All authors have given approval to the final version of the manuscript. A.S.V. and B.S.S. directed the research and edited the manuscript.

Notes

The authors declare no competing financial interest.

■ ACKNOWLEDGMENTS

This material is based upon work supported by the National Science Foundation CHE-1808234. A portion of this work was performed in the McKnight Brain Institute at the National High Magnetic Field Laboratory's Advanced Magnetic Resonance Imaging and Spectroscopy (AMRIS) Facility, which is supported by the National Science Foundation Cooperative Agreement No. DMR-1644779 and the State of Florida. A portion of this work was supported by an NIH award, S10 RR031637, for magnetic resonance instrumentation.

■ REFERENCES

(1) Heeger, A. J. Semiconducting and Metallic Polymers: The Fourth Generation of Polymeric Materials (Nobel Lecture). *Angew. Chem., Int. Ed.* **2001**, *40*, 2591−2611.
(2) MacDiarmid, A. G. "Synthetic Metals": A Novel Role for Organic Polymers (Nobel Lecture). *Angew. Chem., Int. Ed.* **2001**, *40*, 2581−2590.
(3) Shirakawa, H. The Discovery of Polyacetylene Film: The Dawning of an Era of Conducting Polymers (Nobel Lecture). *Angew. Chem., Int. Ed.* **2001**, *40*, 2574−2580.
(4) Chiang, C. K.; Fincher, C. R.; Park, Y. W.; Heeger, A. J.; Shirakawa, H.; Louis, E. J.; Gau, S. C.; Macdiarmid, A. G. Electrical Conductivity in Doped Polyacetylene. *Phys. Rev. Lett.* **1977**, *39*, 1098−1101.
(5) Shirakawa, H.; Louis, E. J.; Macdiarmid, A. G.; Chiang, C. K.; Heeger, A. J. Synthesis of Electrically Conducting Organic Polymers - Halogen Derivatives of Polyacetylene, $(CH)_X$. *J. Chem. Soc.-Chem. Commun.* **1977**, *16*, 578−580.
(6) Moraes, F.; Davidov, D.; Kobayashi, M.; Chung, T. C.; Chen, J.; Heeger, A. J.; Wudl, F. Doped Poly(Thiophene) - Electron-Spin Resonance Determination of the Magnetic-Susceptibility. *Synth. Met.* **1985**, *10*, 169−179.
(7) Chen, J.; Chung, T. C.; Moraes, F.; Heeger, A. J. Soliton Lattice to Metal: A first Order Phase-Transition. *Solid State Commun.* **1985**, *53*, 757−763.
(8) San Jose, B. A.; Matsushita, S.; Moroishi, Y.; Akagi, K. Disubstituted Liquid Crystalline Polyacetylene Derivatives That Exhibit Linearly Polarized Blue and Green Emissions. *Macromolecules* **2011**, *44*, 6288−6302.
(9) Yin, S. C.; Xu, H. Y.; Shi, W. F.; Gao, Y. C.; Song, Y. L.; Wing, J.; Lam, Y.; Tang, B. Z. Synthesis and Optical Properties of Polyacetylenes Containing Nonlinear Optical Chromophores. *Polymer* **2005**, *46*, 7670−7677.
(10) Samuel, I. D. W.; Ledoux, I.; Dhenaut, C.; Zyss, J.; Fox, H. H.; Schrock, R. R.; Silbey, R. J. Saturation of Cubic Optical Nonlinearity in Long-Chain Polyene Oligomers. *Science* **1994**, *265*, 1070−1072.
(11) Tang, B. Z.; Chen, H. Z.; Xu, R. S.; Lam, J. W. Y.; Cheuk, K. K. L.; Wong, H. N. C.; Wang, M. Structure-Property Relationships for Photoconduction in Substituted Polyacetylenes. *Chem. Mater.* **2000**, *12*, 213−221.
(12) Tang, B. Z.; Xu, H. Y.; Lam, J. W. Y.; Lee, P. P. S.; Xu, K. T.; Sun, Q. H.; Cheuk, K. K. L. C-60-Containing Poly(1-Phenyl-1-Alkynes): Synthesis, Light Emission, and Optical Limiting. *Chem. Mater.* **2000**, *12*, 1446−1455.
(13) Hu, Y.; Shiotsuki, M.; Sanda, F.; Freeman, B. D.; Masuda, T. Synthesis and Properties of Indan-Based Polyacetylenes That Feature the Highest Gas Permeability among All the Existing Polymers. *Macromolecules* **2008**, *41*, 8525−8532.
(14) Hu, Y.; Shiotsuki, M.; Sanda, F.; Masuda, T. Synthesis and Extremely High Gas Permeability of Polyacetylenes Containing Polymethylated Indan/Tetrahydronaphthalene Moieties. *Chem. Commun.* **2007**, 4269−4270.
(15) Toy, L. G.; Nagai, K.; Freeman, B. D.; Pinnau, I.; He, Z.; Masuda, T.; Teraguchi, M.; Yampolskii, Y. P. Pure-Gas and Vapor Permeation and Sorption Properties of Poly[1-Phenyl-2-[P-(Trimethylsilyl)Phenyl]Acetylene] (PTMSDPA). *Macromolecules* **2000**, *33*, 2516−2524.
(16) Lam, J. W. Y.; Kong, X.; Dong, Y.; Cheuk, K. K. L.; Xu, K.; Tang, B. Z. Synthesis and Properties of Liquid Crystalline Polyacetylenes with Different Spacer Lengths and Bridge Orientations. *Macromolecules* **2000**, *33*, 5027−5040.
(17) Choi, S.-K.; Lee, J.-H.; Kang, S.-J.; Jin, S.-H. Side-Chain Liquid-Crystalline Poly (1,6-Heptadiyne)s and Other Side-Chain Liquid-Crystalline Polyacetylenes. *Prog. Polym. Sci.* **1997**, *22*, 693−734.
(18) Skotheim, T. A.; Reynolds, J. R., Handbook of Conducting Polymers. *Conjugated Polymers: Theory, Synthesis, Properties, and Characterization*; 3rd ed.; CRC Press: Boca Raton, 2007.
(19) Kang, I.; Yun, H. J.; Chung, D. S.; Kwon, S. K.; Kim, Y. H. Record High Hole Mobility in Polymer Semiconductors Via Side-Chain Engineering. *J. Am. Chem. Soc.* **2013**, *135*, 14896−14899.
(20) Liu, Y. H.; Zhao, J. B.; Li, Z. K.; Mu, C.; Ma, W.; Hu, H. W.; Jiang, K.; Lin, H. R.; Ade, H.; Yan, H. Aggregation and Morphology Control Enables Multiple Cases of High-Efficiency Polymer Solar Cells. *Nat. Commun.* **2014**, *5*, 5293−5298.
(21) Natta, G.; Mazzanti, G.; Corradini, P. Polimerizzazione stereospecifica dell'acetilene. *Atti Accad. Naz. Lincei Rend. CI. Sci. Fis. Mat. Nat.* **1958**, *25*, 3.
(22) Ito, T.; Shirakawa, H.; Ikeda, S. Simultaneous Polymerization and Formation of Polyacetylene Film on the Surface of Concentrated Soluble Ziegler-Type Catalyst Solution. *J. Polym. Sci. Pol. Chem. Ed.* **1974**, *12*, 11−20.
(23) Shirakawa, H.; Ikeda, S. Infrared Spectra of Poly(Acetylene). *Polym. J.* **1971**, *2*, 231−244.
(24) Chiang, C. K.; Druy, M. A.; Gau, S. C.; Heeger, A. J.; Louis, E. J.; Macdiarmid, A. G.; Park, Y. W.; Shirakawa, H. Synthesis of Highly Conducting Films of Derivatives of Polyacetylene, $(CH)_X$. *J. Am. Chem. Soc.* **1978**, *100*, 1013−1015.
(25) Swager, T. M.; Dougherty, D. A.; Grubbs, R. H. Strained Rings as a Source of Unsaturation: Polybenzvalene, a New Soluble Polyacetylene Precursor. *J. Am. Chem. Soc.* **1988**, *110*, 2973−2974.
(26) Chen, Z.; Mercer, J. A. M.; Zhu, X.; Romaniuk, J. A. H.; Pfattner, R.; Cegelski, L.; Martinez, T. J.; Burns, N. Z.; Xia, Y. Mechanochemical Unzipping of Insulating Polyladderene to Semiconducting Polyacetylene. *Science* **2017**, *357*, 475−479.
(27) Yang, J.; Horst, M.; Romaniuk, J. A. H.; Jin, Z.; Cegelski, L.; Xia, Y. Benzoladderene Mechanophores: Synthesis, Polymerization, and Mechanochemical Transformation. *J. Am. Chem. Soc.* **2019**, *141*, 6479−6483.
(28) Su, J. K.; Feist, J. D.; Yang, J.; Mercer, J. A. M.; Romaniuk, J. A. H.; Chen, Z.; Cegelski, L.; Burns, N. Z.; Xia, Y. Synthesis and Mechanochemical Activation of Ladderene-Norbornene Block Copolymers. *J. Am. Chem. Soc.* **2018**, *140*, 12388−12391.

(29) Boswell, B. R.; Mansson, C. M. F.; Cox, J. M.; Jin, Z.; Romaniuk, J. A. H.; Lindquist, K. P.; Cegelski, L.; Xia, Y.; Lopez, S. A.; Burns, N. Z. Mechanochemical Synthesis of an Elusive Fluorinated Polyacetylene. *Nat. Chem.* **2021**, *13*, 41−46.
(30) Seo, J.; Lee, S. Y.; Bielawski, C. W. Unveiling a Masked Polymer of Dewar Benzene Reveals Trans-Poly(Acetylene). *Macromolecules* **2019**, *52*, 2923−2931.
(31) Bott, D. C.; Brown, C. S.; Chai, C. K.; Walker, N. S.; Feast, W. J.; Foot, P. J. S.; Calvert, P. D.; Billingham, N. C.; Friend, R. H. Durham Poly acetylene: Preparation and Properties of the Unoriented Material. *Synth. Met.* **1986**, *14*, 245−269.
(32) Edwards, J. H.; Feast, W. J.; Bott, D. C. New Routes to Conjugated Polymers: 1. A two Step Route to Polyacetylene. *Polymer* **1984**, *25*, 395−398.
(33) Edwards, J. H.; Feast, W. J. A New Synthesis of Poly-(Acetylene). *Polymer* **1980**, *21*, 595−596.
(34) Miao, Z.; Gonsales, S. A.; Ehm, C.; Mentink-Vigier, F.; Bowers, C. R.; Sumerlin, B. S.; Veige, A. S. Cyclic Polyacetylene. *Nat. Chem.* **2021**, *13*, 792−799.
(35) McGowan, K. P.; O'Reilly, M. E.; Ghiviriga, I.; Abboud, K. A.; Veige, A. S. Compelling Mechanistic Data and Identification of the Active Species in Tungsten-Catalyzed Alkyne Polymerizations: Conversion of a Trianionic Pincer into a New Tetraanionic Pincer-Type Ligand. *Chem. Sci.* **2013**, *4*, 1145−1155.
(36) Roland, C. D.; Li, H.; Abboud, K. A.; Wagener, K. B.; Veige, A. S. Cyclic Polymers from Alkynes. *Nat. Chem.* **2016**, *8*, 791−796.
(37) Roland, C. D.; Zhang, T.; VenkatRamani, S.; Ghiviriga, I.; Veige, A. S. A Catalytically Relevant Intermediate in the Synthesis of Cyclic Polymers from Alkynes. *Chem. Commun.* **2019**, *55*, 13697−13700.
(38) Haque, F. M.; Grayson, S. M. The Synthesis, Properties and Potential Applications of Cyclic Polymers. *Nat. Chem.* **2020**, *12*, 433−444.
(39) Niu, W.; Gonsales, S. A.; Kubo, T.; Bentz, K. C.; Pal, D.; Savin, D. A.; Sumerlin, B. S.; Veige, A. S. Polypropylene: Now Available without Chain Ends. *Chem* **2019**, *5*, 237−244.
(40) Miao, Z.; Pal, D.; Niu, W.; Kubo, T.; Sumerlin, B. S.; Veige, A. S. Cyclic Poly(4-Methyl-1-Pentene): Efficient Catalytic Synthesis of a Transparent Cyclic Polymer. *Macromolecules* **2020**, *53*, 7774−7782.
(41) Gonsales, S. A.; Kubo, T.; Flint, M. K.; Abboud, K. A.; Sumerlin, B. S.; Veige, A. S. Highly Tactic Cyclic Polynorbornene: Stereoselective Ring Expansion Metathesis Polymerization of Norbornene Catalyzed by a New Tethered Tungsten-Alkylidene Catalyst. *J. Am. Chem. Soc.* **2016**, *138*, 4996−4999.
(42) Jakhar, V.; Pal, D.; Ghiviriga, I.; Abboud, K. A.; Lester, D. W.; Sumerlin, B. S.; Veige, A. S. Tethered Tungsten-Alkylidenes for the Synthesis of Cyclic Polynorbornene Via Ring Expansion Metathesis: Unprecedented Stereoselectivity and Trapping of Key Catalytic Intermediates. *J. Am. Chem. Soc.* **2021**, *143*, 1235−1246.
(43) Miao, Z.; Kubo, T.; Pal, D.; Sumerlin, B. S.; Veige, A. S. pH-Responsive Water-Soluble Cyclic Polymer. *Macromolecules* **2019**, *52*, 6260−6265.
(44) Yamamoto, T.; Hosokawa, M.; Nakamura, M.; Sato, S. I.; Isono, T.; Tajima, K.; Satoh, T.; Sato, M.; Tezuka, Y.; Saeki, A.; Kikkawa, Y. Synthesis, Isolation, and Properties of All Head-to-Tail Cyclic Poly(3-hexylthiophene): Fully Delocalized Exciton over the Defect-Free Ring Polymer. *Macromolecules* **2018**, *51*, 9284−9293.
(45) Lidster, B. J.; Hirata, S.; Matsuda, S.; Yamamoto, T.; Komanduri, V.; Kumar, D. R.; Tezuka, Y.; Vacha, M.; Turner, M. L. Macrocyclic Poly(*p*-phenylenevinylene)s by Ring Expansion Metathesis Polymerisation and Their Characterisation by Single-molecule Spectroscopy. *Chem. Sci.* **2018**, *9*, 2934−2941.
(46) Basescu, N.; Liu, Z. X.; Moses, D.; Heeger, A. J.; Naarmann, H.; Theophilou, N. High Electrical Conductivity in Doped Polyacetylene. *Nature* **1987**, *327*, 403−405.
(47) Tsukamoto, J.; Takahashi, A. Synthesis and Electrical-Properties of Polyacetylene Yielding Conductivity of 10^5 S/cm. *Synth. Met.* **1991**, *41*, 7−12.
(48) Pal, D.; Miao, Z.; Garrison, J. B.; Veige, A. S.; Sumerlin, B. S. Ultra-high-Molecular-Weight Macrocyclic Bottlebrushes Via Post-Polymerization Modification of a Cyclic Polymer. *Macromolecules* **2020**, *53*, 9717−9724.
(49) Sarkar, S.; McGowan, K. P.; Kuppuswamy, S.; Ghiviriga, I.; Abboud, K. A.; Veige, A. S. An OCO^{3-} Trianionic Pincer Tungsten(Vi) Alkylidyne: Rational Design of a Highly Active Alkyne Polymerization Catalyst. *J. Am. Chem. Soc.* **2012**, *134*, 4509−4512.
(50) Nadif, S. S.; Kubo, T.; Gonsales, S. A.; VenkatRamani, S.; Ghiviriga, I.; Sumerlin, B. S.; Veige, A. S. Introducing "Ynene" Metathesis: Ring-Expansion Metathesis Polymerization Leads to Highly Cis and Syndiotactic Cyclic Polymers of Norbornene. *J. Am. Chem. Soc.* **2016**, *138*, 6408−6411.
(51) Roovers, J. Dilute-Solution Properties of Ring Polystyrenes. *J. Polym. Sci.: Polym. Phys. Ed.* **1985**, *23*, 1117−1126.
(52) Sun, P.; Liu, J.'. A.; Zhang, Z.; Zhang, K. Scalable Preparation of Cyclic Polymers by the Ring-Closure Method Assisted by the Continuous-Flow Technique. *Polym. Chem.* **2016**, *7*, 2239−2244.
(53) Jeong, Y.; Jin, Y.; Chang, T.; Uhlik, F.; Roovers, J. Intrinsic Viscosity of Cyclic Polystyrene. *Macromolecules* **2017**, *50*, 7770−7776.
(54) Bloomfie, V.; Zimm, B. H. Viscosity Sedimentation Et Cetera of Ring- and Straight-Chain Polymers in Dilute Solution. *J. Chem. Phys.* **1966**, *44*, 315−323.
(55) Shirakawa, H.; Ito, T.; Ikeda, S. Raman Scattering and Electronic-Spectra of Poly(Acetylene). *Polym. J.* **1973**, *4*, 460−462.
(56) Lichtmann, L. S.; Fitchen, D. B.; Temkin, H. Resonant Raman-Spectroscopy of Conducting Organic Polymers - $(CH)_X$, and an Oriented Analog. *Synth. Met.* **1980**, *1*, 139−149.
(57) Chance, R. R.; Schaffer, H.; Knoll, K.; Schrock, R.; Silbey, R. Linear Optical Properties of a Series of Linear Polyenes: Implications for Polyacetylene. *Synth. Met.* **1992**, *49*, 271−280.
(58) Schaffer, H. E.; Chance, R. R.; Silbey, R. J.; Knoll, K.; Schrock, R. R. Conjugation Length Dependence of Raman Scattering in a Series of Linear Polyenes: Implications for Polyacetylene. *J. Chem. Phys.* **1991**, *94*, 4161−4170.
(59) Schaffer, H.; Chance, R.; Knoll, K.; Schrock, R.; Silbey, R., Linear Optical Properties of a Series of Polyacetylene Oligomers. In *Conjugated Polymeric Materials: Opportunities in Electronics, Optoelectronics, and Molecular Electronics*; Springer: 1990; 365−376.
(60) Schügerl, F. B.; Kuzmany, H. Optical Modes of trans-Polyacetylene. *J. Chem. Phys.* **1981**, *74*, 953−958.
(61) Brivio, G. P.; Mulazzi, E. Theoretical Analysis of Absorption and Resonant Raman Scattering Spectra of trans-$(CH)_X$. *Phys. Rev. B* **1984**, *30*, 876−882.

https://doi.org/10.1021/acs.macromol.1c00938
Macromolecules 2021, 54, 7840−7848